Multispectral Satellite-to-In-Situ Comparison Uncertainty Budget

Author: _____ ***Samantha Malone***
NPL, Task Technical Expert

Reviewer: _____ ***Sam Hunt***
NPL, Task Leader

Issue: 1.0
Date: 31/01/2026

© NPL Management Limited, 2026

The copyright in this document is vested in NPL Management Ltd.

This document may only be reproduced in whole or in part, or stored in a retrieval system, or transmitted in any form, or by any means electronic, mechanical, photocopying or otherwise, either with the prior permission of NPL Management Ltd. or in accordance with the terms of Contract referenced CW 322785 and dated 15/12/2020.

Authors

Samantha Malone, Maddie Stedman, Sam Hunt, Harry Morris, Joe Riordan, Pieter De Vis

National Physical Laboratory

Hampton Road, Teddington, Middlesex, TW11 0LW

This report is NPL - Commercial and must not be exposed to casual examination. It is not for general distribution and should not be cited as a reference other than in accordance with the contract.

Contents

1 Introduction 3
1.1 Scope 3
1.2 Changes Log 3
1.3 Reference Documents 3
1.4 Acronyms & Abbreviations 4
2 Overview of approach 6
2.1 Principles of Uncertainty Analysis 6
2.1.1 Analytical Uncertainty Propagation 7
2.1.2 Numerical Uncertainty Propagation 7
2.1.3 Error-Correlation in Measurement Series 7
2.2 QA4EO Uncertainty Analysis Framework 9
2.2.1 Measurement Function Based Analysis 10
2.2.2 Effects Tables Reporting 10
3 Description of Sensors and Comparison Approach 12
3.1 Reference and Target Sensors Involved 12
3.2 Multispectral Satellite-to-In-Situ Comparison Approach 13
4 Comparison Measurement Function Analysis 15
4.1 Multispectral Satellite-to-In-Situ Comparison 15
4.1.1 Satellite Product Processing 15
4.1.1.1 Spatial Aggregation 15
4.1.2 Reference Product Processing 16
4.1.2.1 Spectral Band Integration 16
4.1.2.2 Temporal Interpolation 16
4.2 Uncertainty Tree Diagram 17
5 Discussion of Uncertainty Contributions 18
5.1 Satellite Sensor Effects 18
5.2 Reference Data Effects 19
5.3 Comparison Process Effects 21
5.3.1 Spatial Aggregation Method Effects 21
5.3.2 Observation Geometry Difference Effects 23
5.3.3 Band Integration Method Effects 27
5.3.3.1 Target sensor spectral calibration uncertainty 27

5.3.3.2 Spectral resolution of the reference data 28
5.3.3.3 Effects Table 29
5.3.4 Temporal Interpolation Model Effect 30
5.4 Combining the comparison uncertainties 31
6 Discussion 32

1 Introduction

1.1 Scope

This document provides the metrologically derived and described uncertainty budget for multispectral satellite-to-in-situ comparisons and serves as the basis for the uncertainty evaluation underpinning the RadVal tool of the CEOS-PVP.

The document begins with an introduction to the approach and methodology used in the study, in Section 2. This is followed by Section 3, which describes how the comparisons are carried out and of the sensors involved. Further details of the comparison measurement functions are outlined in Section 0 with an associated uncertainty tree diagram in Section 4.2. The identified uncertainty effects are discussed in Section 5, with associated effects tables. Finally, Section 6 includes a discussion around the identified uncertainties and information on next steps to mature the evaluation of corresponding magnitude of the effects.

1.2 Changes Log

Issue	Date	Description
1.0	31/01/2026	Preliminary version

1.3 Reference Documents

[RD-1]	JCGM 100:2008 Evaluation of measurement data – Guide to the expression of uncertainty in measurement, Report (http://www.bipm.org/en/publications/guides)
[RD-2]	JCGM (2008). "Evaluation of measurement data — Supplement 1 to the "Guide to the expression of uncertainty in measurement" — Propagation of distributions using a Monte Carlo method" (*JGCM*, vol. 101, 2008)
[RD-3]	JCGM 200:2008 International vocabulary of metrology - basic and general concepts and associated terms (http://www.bipm.org/en/publications/guides)
[RD-4]	Woolliams et al. (2017), FIDUCEO Project Technical Document – D2.2a Principles behind the FCDR effects table
[RD-5]	Mittaz et al. (2018), FIDUCEO Project Technical Document – D2.2d Report on the AVHRR FCDR: Uncertainty
[RD-6]	Mittaz, J., Merchant, C. J., & Woolliams, E. R. (2019), Applying principles of metrology to historical Earth observations from satellites. *Metrologia*, *56*(3), 032002.
[RD-7]	Woolliams, E. *et al.* (2025) 'A Metrological Framework for Addressing Uncertainty in Satellite and In Situ Earth Environmental Observations', *Surveys in Geophysics* [Preprint]. Available at: https://doi.org/10.1007/s10712-025-09916-5
[RD-8]	https://www.radcalnet.org/resources/RadCalNetQuickstartGuide_20180702.pdf
[RD-9]	RadCalNet Portal. Available at: www.radcalnet.org (Last Accessed 31/03/2026)
[RD-10]	SentiWiki. Overview of Sentinel-2 Mission. Available at: https://sentiwiki.copernicus.eu/web/s2-mission (Last Accessed 31/03/2026)
[RD-11]	Collison, A., Jumpasut, A., & Bourne, H. (2022). On-orbit radiometric calibration of the Planet satellite fleet: Doves and SkySats. *Planet Labs White Paper*, 1–40.

[RD-12]	S2 MSI ESL Team. (2025). *Sentinel-2 L1C MSI Data Quality Report – June 2025* (Issue 112). Copernicus Space Component Mission Performance Cluster Service / ESA. Ref. OMPC.CS.DQR.01.05-2025.
[RD-13]	Gorroño, J.; Fomferra, N.; Peters, M.; Gascon, F.; Underwood, C.I.; Fox, N.P.; Kirches, G.; Brockmann, C. A Radiometric Uncertainty Tool for the Sentinel 2 Mission. Remote Sens. 2017, 9, 178. https://doi.org/10.3390/rs9020178
[RD-14]	Bouvet, M.; Thome, K.; Berthelot, B.; Bialek, A.; Czapla-Myers, J.; Fox, N.P.; Goryl, P.; Henry, P.; Ma, L.; Marcq, S.; et al. RadCalNet: A Radiometric Calibration Network for Earth Observing Imagers Operating in the Visible to Shortwave Infrared Spectral Range. Remote Sens. 2019, 11, 2401. https://doi.org/10.3390/rs11202401
[RD-15]	*Landier, L., Meygret, A. (2022)* RadCalNet Uncertainty Statement – Gobabeb: QA4EO-WGCV-RadCalNet-GONA-U-v2. Available through the RadCalNet portal.
[RD-16]	Sinclair, M. *BRDF Model Fitting Using In-Situ Dataset Over LANDHYPERNET Satellite Calibration Site (Gobabeb, Namibia).* Manuscript in prep.
[RD-17]	https://www.comet-toolkit.org/ De Vis & Hunt. *CoMet Toolkit (Community Metrology Toolkit).* Manuscript in prep.
[RD-18]	Meerdink, Susan K., et al. "The ECOSTRESS spectral library version 1.0." Remote Sensing of Environment 230 (2019): 111196.
[RD-19]	Kokaly, Raymond F., et al. USGS spectral library version 7. No. 1035. US Geological Survey, 2017.
[RD-20]	PICSAND Spectral Library.
[RD-21]	C. Emde, "The libradtran software package for radiative transfer calculations (version 2.0. 1)," Geosci. Model Develop., vol. 9, no. 5, pp. 1647–1672, 2016.
[RD-22]	Szantoi, Zoltan, and Peter Strobl. "Copernicus Sentinel-2 calibration and validation." European Journal of Remote Sensing 52.1 (2019): 253-255.

1.4 Acronyms & Abbreviations

AVHRR	Advanced Very High Resolution Radiometer
BOA	Bottom-of-Atmosphere
BRDF	Bidirectional Reflectance Distribution Function
CEOS	Committee on Earth Observation Satellites
CoMet	Community Metrology Toolkit
EO	Earth Observation
ESA	European Space Agency
(F)CDR	(Fundamental) Climate Data Record
FIDUCEO	Fidelity and uncertainty in climate data records from Earth observations – European Union Horizon 2020 Project
FOV	Field-of-View
GONA	Gobabeb, Namibia (RCN site code)
GHNA	HYPERNETS Gobabeb site
GUM	Guide to the expression of uncertainty in measurement
L1	Level 1 Data – calibrated top-of-atmosphere radiance or reflectance
MCM	Monte Carlo Method
MSI	Multi-Spectral Instrument
NPL	National Physical Laboratory
OLI	Operational Land Imager
PDF	Probability Density Function
PICS	Pseudo-invariant Calibration Site

QA4EO	Quality Assurance Framework for Earth Observation
RCN	RadCalNet – Radiometric Calibration Network
RVUS	Railroad Valley, USA (RCN site code)
SI	International System of Units
SRF	Spectral Response Function
TOA	Top-of-Atmosphere
UTM	Universal Transverse Mercator projection
VIM	International Vocabulary of Metrology
WGCV	Working Group on Calibration and Validation (CEOS)

2 Overview of approach

The following section provides an overview of the approach used for the uncertainty analysis in this report. It is based on the approach defined in [RD-4, RD-5, RD-6, RD-7].

2.1 Principles of Uncertainty Analysis

The Guide to the expression of Uncertainty in Measurement (GUM) [RD-1] provides an internationally accepted framework for how to determine and express the uncertainty of the measured value of a given measurand (the quantity which is being measured). The International Vocabulary of Metrology (VIM) [RD-3] defines measurement uncertainty as:

"a non-negative parameter characterizing the dispersion of the quantity values being attributed to a measurand, based on the information used."

The standard uncertainty is the measurement uncertainty expressed as a standard deviation. Please note this is a separate concept to measurement error, which is also defined in the VIM as:

"the measured quantity value minus a reference quantity value."

Generally, the "reference quantity" is considered to be the "true value" of the measurand and is therefore unknown. Figure 1 illustrates these concepts.

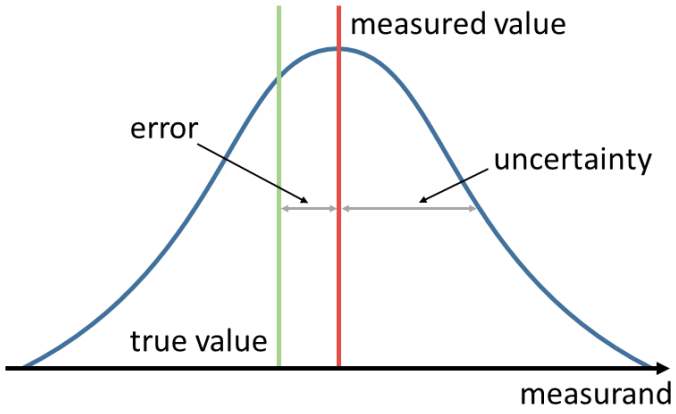


Figure 1 – Dia gram illustrating the different concepts of measured value and true value, uncertainty and error

Within the GUM framework uncertainty analysis begins with understanding the measurement function. The measurement function establishes the mathematical relationship between all known input quantities (e.g. instrument counts) and the measurand itself (e.g. radiance). Generally, this may be written as,

$$Y = f(X_1, \ldots, X_N), \qquad \textit{Equation 1}$$

where:

- Y is the measurand;
- X_i are the input quantities.

The measurement function for multispectral satellite-to-in-situ comparisons is defined in Section 0.

Uncertainty analysis is then performed by considering in turn each of these different input quantities to the measurement function, this process is represented in Figure 2. Each input quantity may be influenced by one or more error effects which are described by an uncertainty distribution. Each uncertainty component for the multispectral satellite-to-in-situ comparisons is defined in Section 5.

These separate distributions may then be combined to determine the uncertainty of the measurand, $u^2(Y)$. This may be achieved analytically or numerically, as described in the following sections.

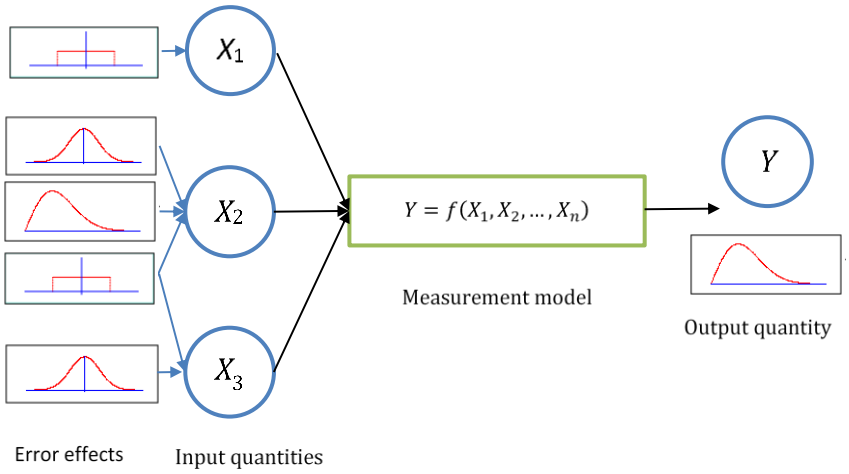


Figure 2 – Conceptual process of uncertainty propagation

2.1.1 Analytical Uncertainty Propagation

Analytical uncertainty propagation is performed using the so-called *Law of Propagation of Uncertainties* [RD-1],

$$u^2(Y) = \boldsymbol{C}\boldsymbol{U}\boldsymbol{C}^T, \qquad \textit{Equation 2}$$

where:

- $\boldsymbol{C}$ is the vector of sensitivity coefficients, $\partial Y/\partial X_i$;
- $\boldsymbol{U}$ is the error covariance matrix for the input quantities.

2.1.2 Numerical Uncertainty Propagation

Numerical methods offer an alternative to the analytical approach for uncertainty propagation, commonly referred to as the Monte Carlo Method (MCM), the best practice for this approach is defined in GUM Supplement 1 [RD-2].

2.1.3 Error-Correlation in Measurement Series

In a series of measurements (for example reflectance values per band for a satellite sensor in a matchup) it is important to consider how the errors between the measurements in the series are correlated. This is crucial when evaluating the uncertainty of a result derived from these data (for example, computing the average bias in a set of comparison between these measurements and in-situ measurements). Typically, three broad categories of error correlation are defined to describe the

correlation structure – random, systematic and structured random. They were first defined by the Horizon 2020 FIDUCEO[1] (Fidelity and uncertainty in climate data records from Earth observations) project [RD-6] as follows:

- **Random effects** – *"those causing errors that cannot be corrected for in a single measured value, even in principle, because the effect is stochastic. Random effects for a particular measurement process vary unpredictably from (one set of) measurement(s) to (another set of) measurement(s). These produce random errors which are entirely uncorrelated between measurements (or sets of measurements) and generally are reduced by averaging."*
- **Systematic (or common) effects** – *"those for a particular measurement process that do not vary (or vary coherently) from (one set of) measurement(s) to (another set of) measurement(s) and therefore produce systematic errors that cannot be reduced by averaging."*
- **Structured random effects – "***means that across many observations there is a deterministic pattern of errors whose amplitude is stochastically drawn from an underlying probability distribution; "structured random" therefore implies "unpredictable" and "correlated across measurements"."*

These correlation types are sufficient to describe the error correlation across the relevant correlation scales.

Examples of errors with the different error-correlation structures identified above, and their corresponding error-correlation matrices, are illustrated in Figure 3. The first column shows random error, sometimes referred to as independent due to the lack of error-correlation between pixels. The second column shows an example of structured random error-correlation pattern – here errors are fully correlated between pixels in each row, but random between rows. The third column illustrates a systematic effect, here you have the same error in every pixel. The final column shows the combination of each of these effects to give a total error.

[1] See: https://research.reading.ac.uk/fiduceo/

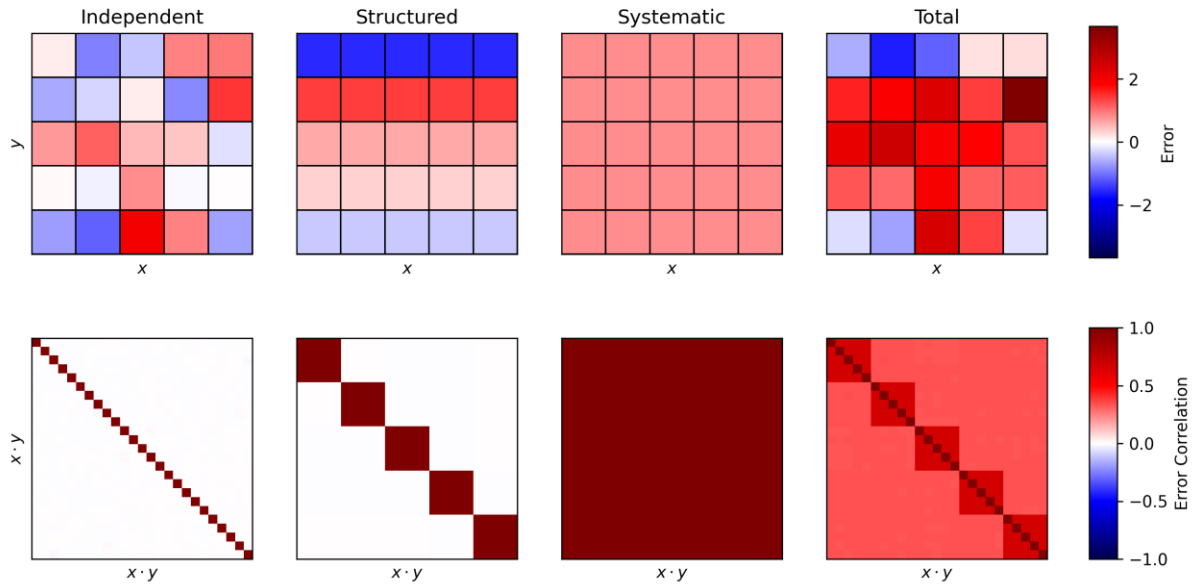


Figure 3 – Top row - examples of errors with independent (random), structured and systematic error-correlation structures, and the total combined error. Bottom row - the corresponding error correlation matrix for each error from the top row

2.2 QA4EO Uncertainty Analysis Framework

Within the FIDUCEO project a framework was developed to apply rigorous GUM-based metrological methods to satellite sensor fundamental climate data records (FCDRs) to provide per pixel uncertainties [RD-5]. This has since been developed within the QA4EO framework, which defined a step-by-step systematic approach, the 'QA4EO Five Steps' to uncertainty analysis, allowing the process to be more achievable by any EO mission [RD-7]. In this document this approach is applied to multispectral satellite-to-in-situ comparisons, providing a detailed uncertainty analysis for these comparisons. The fundamentals of this approach are described in this section.

2.2.1 Measurement Function Based Analysis

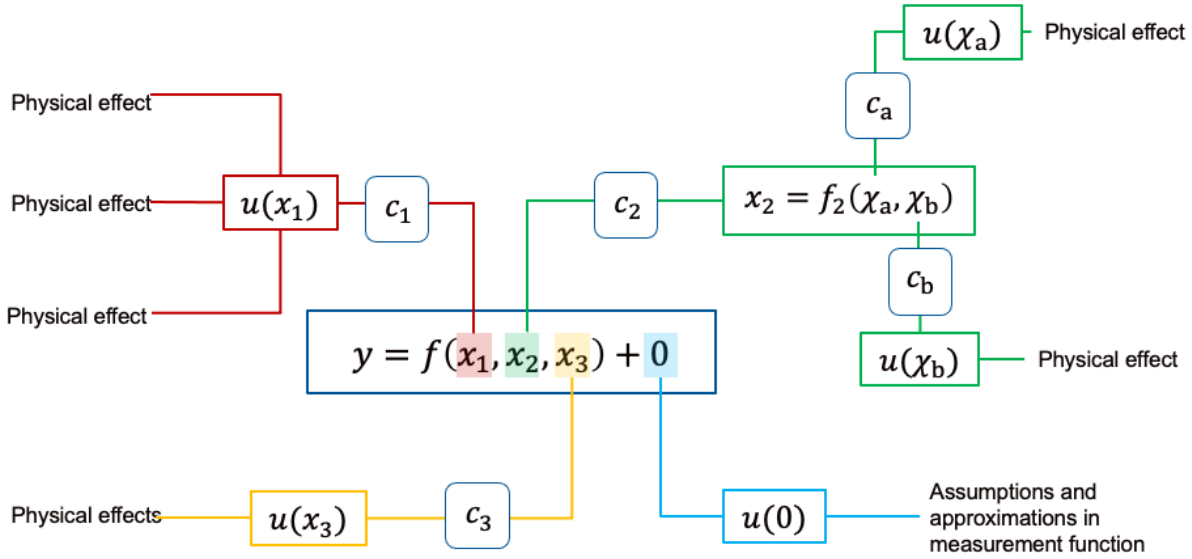


Figure 4 – Generic example of an uncertainty tree diagram

As described in Section 2.1, the basis of any metrologically rigorous measurement is to firstly understand how the measurand (e.g., reflectance bias) is determined from a set of input quantities (e.g., per-band reflectance) through a measurement function. Within the FIDUCEO project a schematic representation of the sensor measurement function, called the *uncertainty tree diagram*, formed the basis of the analysis made.

Figure 4 provides a generic uncertainty tree diagram. At the centre of this diagram is the measurement function for the sensor – here with measurand, y, and input quantities, x_1, x_2, and x_3. From this function branches spread from each input quantity, which may themselves be determined by their own measurement functions (for example, here x_2 is evaluated from a measurement function of χ_a and χ_b), to their uncertainty. This uncertainty can be traced back through to its impact on the measurand by the sensitivity coefficients on each branch. Finally, the effects which cause each respective uncertainty are connected to the end of each branch.

Note that we should also consider the extent to which the measurement function describes the true physics of the measurement – this is accounted for by including the term $+0$ at the end of the measurement function. This explicitly represents effects, expected to have zero mean, that are not captured by the measurement function (i.e. there is an uncertainty associated with this quantity being zero).

2.2.2 Effects Tables Reporting

Each of the effects identified at the end of each of the branches should then be understood, quantified and reported in an "Effects Table" which documents:

- The uncertainty associated with the given effect.
- The sensitivity coefficient required to propagate uncertainties associated with that effect to the uncertainty associated with the measurand.

- The correlation structure over band and temporal scales for errors from this effect.

Table 2-1 shows an amended FIDUCEO "Effects Table", with description of how it should be populated. This is adapted from the standard FIDUCEO format [RD-4]. All the error-correlation structures within this report are defined per dimension as either random or systematic.

For multispectral satellite-to-in-situ sensor comparisons error-correlation dimensions are defined as:

- Temporal (within site), t – along the time series of comparisons, for one site
- Band (within site), b – along the spectral bands of the multispectral satellite sensor, for one site
- Between sites, s – between in-situ sites

Table 2-1 Table for codifying the uncertainty due to an error effect and its correlation structure

Table descriptor		How this is codified
Name of effect		A unique name for each source of uncertainty in a term of the measurement function
Affected term in measurement function		Name and standard symbol of affected term
Correlation type and form	Temporal (within site) (t)	Correlation structure at each of the relevant scales.
	Band (within site) (b)	
	Between sites (s)	
Correlation scale	Temporal (within site) (t)	Correlation scale for each of the correlation types
	Band (within site) (b)	
	Between sites (s)	
Uncertainty	PDF shape	Functional form of estimated error distribution for the term
	units	Units in which PDF shape is expressed (units of term, or can be as percentage etc)
	magnitude	Value(s) or parameterisation estimating width of PDF
Sensitivity coefficient		Value, equation or parameterisation of sensitivity of measurand to term

3 Description of Sensors and Comparison Approach

This section describes the specific in-situ reference and target satellite sensors involved in the comparisons this uncertainty budget is defined for, as well as the multispectral satellite–in-situ comparison approach itself.

3.1 Reference and Target Sensors Involved

For the comparisons considered in this uncertainty budget, the reference is RadCalNet (RCN) data collected from the various RCN sites, including GONA (Gobabeb, Namibia) and RVUS (Railroad Valley, USA). For each site, BOA reflectance data is collected and processed through the same central processing chain to obtain TOA reflectances at nadir viewing. The RCN product covers a spectral range of around 400-1000 nm at a 10 nm sampling interval, provided every 30 minutes between 9 am – 3 pm local time (only cloud-free data is made available) [RD-8]. RCN data products have a detailed uncertainty budget, called Uncertainty Statement, per site for the BOA data, available through creating an account on the RCN Portal [RD-9], and the product provides one uncertainty value to represent all sources of error that contribute to the TOA reflectances. Other atmospheric parameter data provided with the product, such as aerosol optical depth, pressure and ozone, also come with their own corresponding uncertainties. To illustrate the general homogeneity of the sites, Figure 5 shows Sentinel-2 data captured over two RCN sites GONA (left) and RVUS (right). In these plots, some small roads are visible, and it is possible to see how the overall reflectance varies between sites.

The target satellite sensors used for these comparisons are those from multispectral EO missions, with the public sector Sentinel-2 Multi-Spectral Instrument (MSI), the Operational Land Imager (OLI) onboard both Landsat 8 and 9 [RD-10, RD-12] used as representative examples throughout this document. However, it should be noted that the analysis is applicable to any similar multi-spectral optical EO imager

3.2 Multispectral Satellite-to-In-Situ Comparison Approach

These satellite-to-in-situ comparisons are the basis for Cal/Val activities utilised by both commercial and space agency missions. See, for example, Planet's radiometric calibration of the SuperDove instrument, which uses multiple RCN sites to validate in-orbit calibration [RD-11].

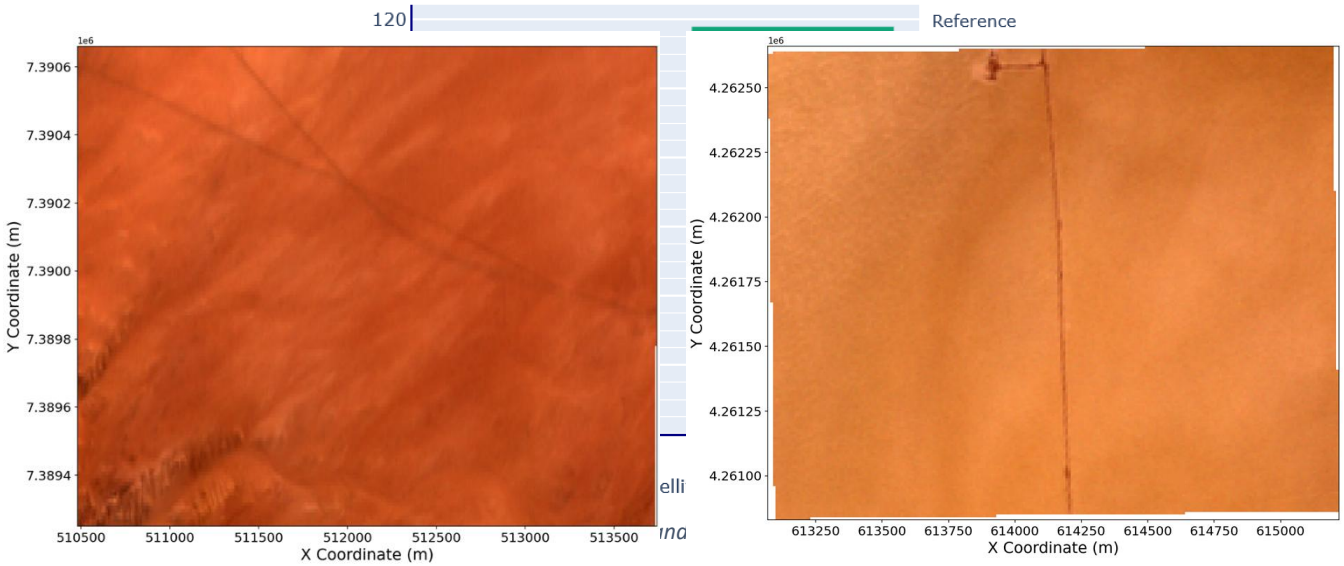


Figure 5 – RGB plots of Sentinel-2 data captured over two RCN sites: GONA (left), RVUS (right), from June 2024.

A matchup is defined here as an overpass of a satellite with a reference site, where both the satellite sensor and RCN acquired data. Figure 6 shows the number of matchups for Sentinel-2 and Landsat over two RCN sites, GONA and RVUS, during 2024. In this case, a matchup is defined as an overpass of the RCN site, with ≤ 15-minute time difference between the overpass and RCN data collection; viewing angles for Landsat at both sites is near-nadir but Sentinel-2 views at a 5˚ angle at GONA and at 10˚ over RVUS and this deviation from nadir for the purpose of this analysis is uncorrected. Disparities in numbers of matchups between sites and satellites is caused, for example, due to cloud cover or site

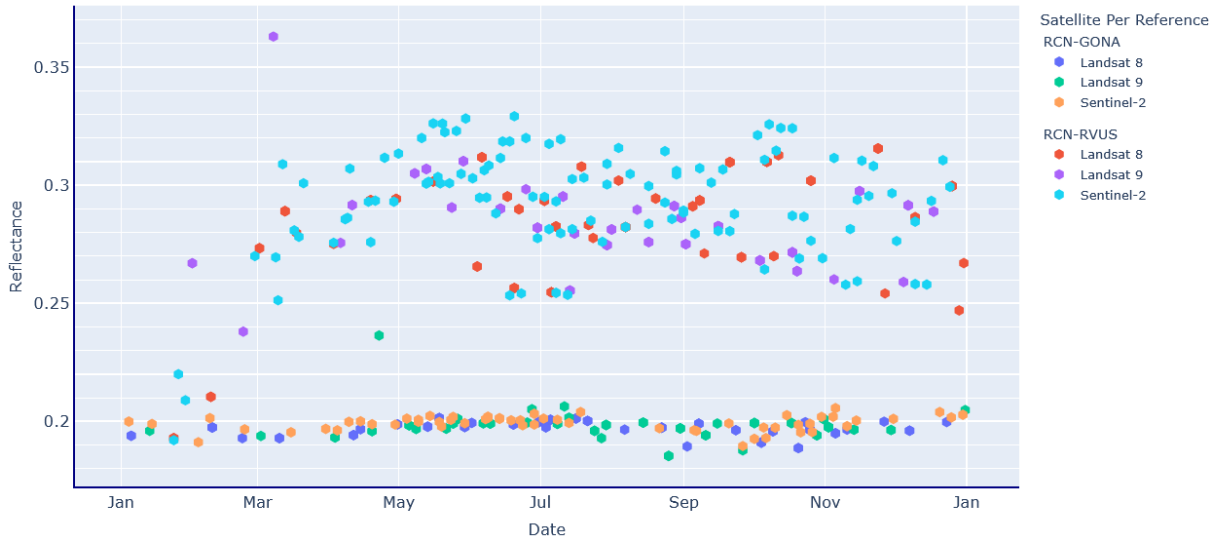


Figure 6 – Satellite L1 TOA reflectances for Sentinel-2 and Landsat 8 and 9 for both RCN sites: GONA & RVUS, between 2022-24 inclusive for the blue band.

up time. Overall, this plot demonstrates the sheer number of matchups to be had with satellites of a temporal resolution of 5 days for Sentinel-2 constellation and 16 days for each Landsat platform.

Figure 7 plots the satellite L1 TOA reflectance measurements for both Sentinel-2 and Landsat in their blue bands over both sites, spanning three years, showing how the measurements vary depending on the site, as RVUS is overall brighter, with GONA more stable over time. This demonstrates how each of the RCN sites have different characteristics, and multispectral satellite comparisons should at least initially be considered individually for each site.

The comparisons entail calculating the bias between satellite measurements and the reference in-situ measurements, allowing monitoring of satellite sensor performance. An example of these results is shown in Figure 8 showing a timeseries of the percentage radiometric bias relevant to the site, for Sentinel-2 over both GONA and RVUS in 2022. This displays how the satellite data varies over time with regards to the site and is therefore a measure of its radiometric stability compared to RCN. Fully understanding the uncertainty budget of the multispectral satellite–in-situ comparisons allows a better characterisation of the uncertainties for Cal/Val activities using these comparisons or for any further research that relies on these comparisons as a basis.

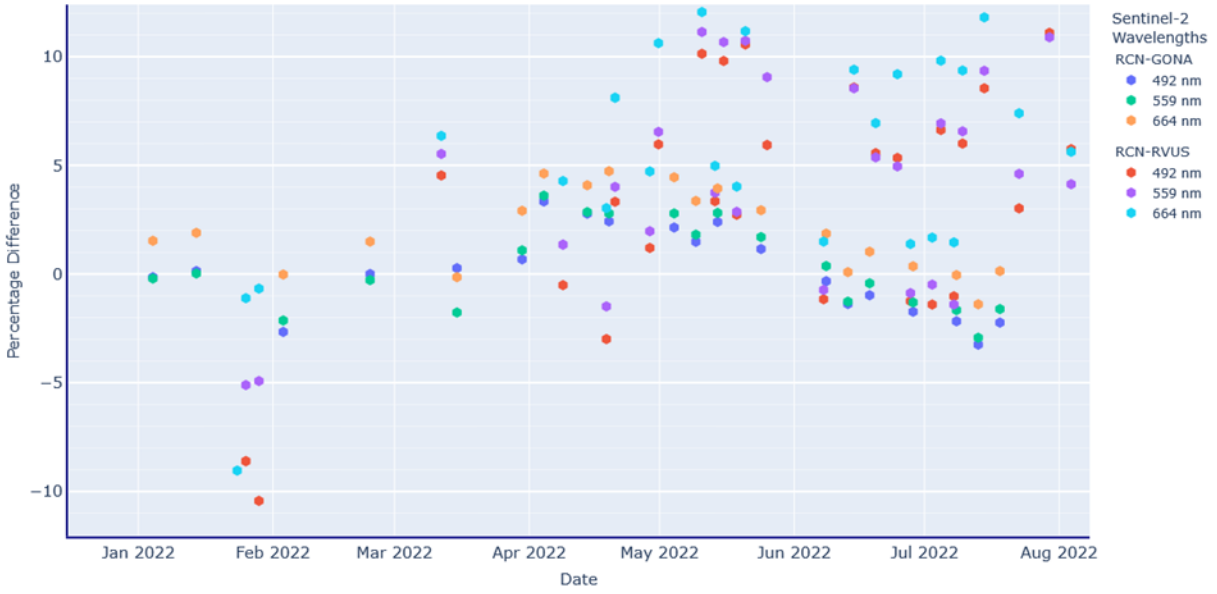


Figure 8 – Example of comparison results for Sentinel-2 data, for the RGB bands, over two RCN sites for 8 months in 2022.

4 Comparison Measurement Function Analysis

In this section the measurement function for multispectral satellite-to-in-situ comparisons is defined. This includes processing to compensate for mismatches between the target and the reference measurements, including spectral band, acquisition time and spatial differences.

Following this, the associated uncertainty tree diagram is defined, to display each of the contributing uncertainty sources to the multispectral satellite-to-in-situ comparison function.

4.1 Multispectral Satellite-to-In-Situ Comparison

The multispectral satellite-to-in-situ comparison function defines the proportional bias between the satellite sensor (target) and the in-situ reference data (ref), relative to the reference. The closer the resulting values are to zero, the closer the satellite sensor and the in-situ reference measurements agree.

The TOA reflectance bias between the target and reference, $\delta\rho_{\text{target,ref}}$, is therefore defined by:

$$\delta\rho_{\text{target,ref}}(\lambda_b, t_{\text{target}}) = \frac{\overline{\rho}_{\text{target}}(\lambda_b, t_{\text{target}}) - \rho_{\text{ref}}(\lambda_b, t_{\text{target}})}{\rho_{\text{ref}}(\lambda_b, t_{\text{target}})} \qquad \textit{Equation 3}$$

where:

- $\overline{\rho}_{\text{target}}(\lambda_b, t_{\text{target}})$ is the spatially aggregated target L1 TOA reflectance at wavelength per band, λ_b, and target time, t_{target}
- $\rho_{\text{ref}}(\lambda_b, t_{\text{target}})$ is the processed reference TOA reflectance at wavelength per satellite band, λ_b, and at target time, t_{target}. This is calculated through multi-step processing of spectral band integration and temporal interpolation.

The following sub-sections explain how these two terms are calculated.

4.1.1 Satellite Product Processing

To enable comparison between the satellite product image and the in-situ point data, the satellite target data needs to be spatially aggregated to match the region of interest (ROI) that the in-situ point measurement is considered to be representative of; this is possible due to the relatively good homogeneity of RCN sites.

4.1.1.1 Spatial Aggregation

For these comparisons, the satellite target data is averaged over the pixels in the ROI to match the reference point data, and therefore the spatially aggregated reflectance values, $\overline{\rho}_{\text{target}}(\lambda_b, t_{\text{target}})$, are defined by the following:

$$\overline{\rho}_{target}(\lambda_b, t_{target}) = \frac{1}{n}\sum_{i=1}^{n} \rho_{target,i}(\lambda_b, t_{target}) \qquad \textit{Equation 4}$$

where:

- $\rho_{\text{target,i}}(\lambda_b, t_{\text{target}})$ are the per-band reflectance values for each satellite pixel within the ROI, i,at the target time, t_{target}
- n is the number of pixels in the satellite image that are averaged

4.1.2 Reference Product Processing

To enable comparison between the hyperspectral in-situ data and the multispectral satellite product, the reference data needs to be spectrally band integrated to match the bands of the target sensor. In addition, the in-situ data needs to be temporally interpolated to match the satellite overpass time.

4.1.2.1 Spectral Band Integration

Given that RCN is a hyperspectral reference, over the same spectral range the in-situ data will typically have a higher resolution than the target sensor; for example, RCN has a spectral range of at least 400-1000 nm at a 10 nm sampling interval [RD-8], compared to Sentinel-2's 12 bands with bandwidth ranging from 14-179 nm [RD-10]. For these comparisons, the reference data spectrum is integrated to match the bands of the target, using its Spectral Response Functions (SRFs). The spectrally integrated reflectance values, $\rho_{\text{ref}}(\lambda_b, \underline{t})$, are defined by the following:

$$\rho_{\text{ref}}(\lambda_b, \underline{t}) = \frac{\int R_b(\lambda)\, \rho_{\text{ref}}(\underline{\lambda}, \underline{t})\, d\lambda}{\int R_b(\lambda)\, d\lambda} \qquad \textit{Equation 5}$$

where:

- $R_b(\lambda)$ is the target response per band, b, at wavelength, λ
- $\rho_{\text{ref}}(\underline{\lambda}, \underline{t})$ is the reference reflectance at all wavelengths, $\underline{\lambda}$, and all times, $\underline{t}$

4.1.2.2 Temporal Interpolation

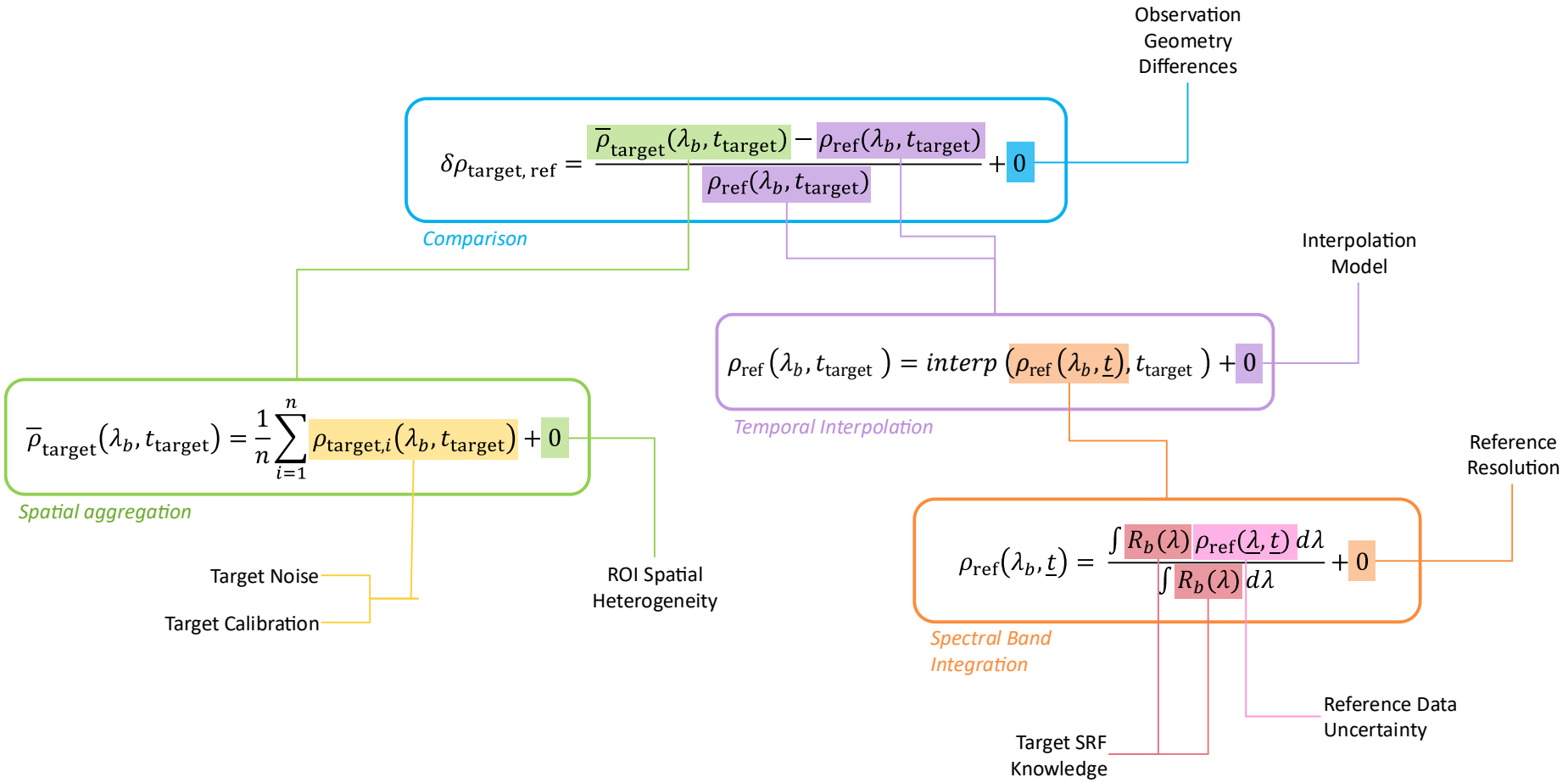
There is typically a non-negligible difference between the time of the satellite overpass and reference in-situ measurement acquisition, given that the RCN product provides data every 30 minutes between 9 am – 3 pm local time (and then only cloud-free data is made available) [RD-8]. To mitigate for this mismatch, the reference in-situ data is linearly interpolated to match the target acquisition time, to obtain the reference reflectances at target time, $\rho_{\text{ref}}(\lambda_b, t_{\text{target}})$, as follows:

$$\rho_{ref}(\lambda_b, t_{target}) = interp\left(\rho_{ref}(\lambda_b, \underline{t}), t_{target}\right) \qquad \textit{Equation 6}$$

where:

- $\rho_{\text{ref}}(\lambda_b, \underline{t})$ are the spectrally integrated reflectance values, from Equation 5
- t_{target} is the target acquisition time

4.2 Uncertainty Tree Diagram



5 Discussion of Uncertainty Contributions

In this section each source of uncertainty identified in the Uncertainty Tree Diagram in Section 4.2 is analysed using an Effects Table following the process outlined in Section 2.2.2.

5.1 Satellite Sensor Effects

This section describes the error effects related to the satellite sensor product. Uncertainty components can vary between satellite products, though commonly include at least noise and calibration.

The noise in satellite measurements sensors can originate from various parts of the processing chain, including photon noise, detector noise, readout noise, and data transmission errors; overall sensor noise will be due to a combination of these various sources. Though the uncertainties due to the sensor vary per band and are dependent on the surface being measured, the uncertainty attributed to overall sensor noise and calibration should be well-defined in the satellite data provider's documentation. The Sentinel-2 Radiometric Uncertainty Tool (RUT) [RD-13] was used to calculate this uncertainty for a given Sentinel-2 tile over the RCN GONA site. This uncertainty encompasses various random and systematic sources of uncertainty arising from the sensor, including straylight, diffuser knowledge and instrument noise. Figure 9 shows this noise uncertainty for the RGB bands, where the maximum is < ~0.75 % for the blue band.

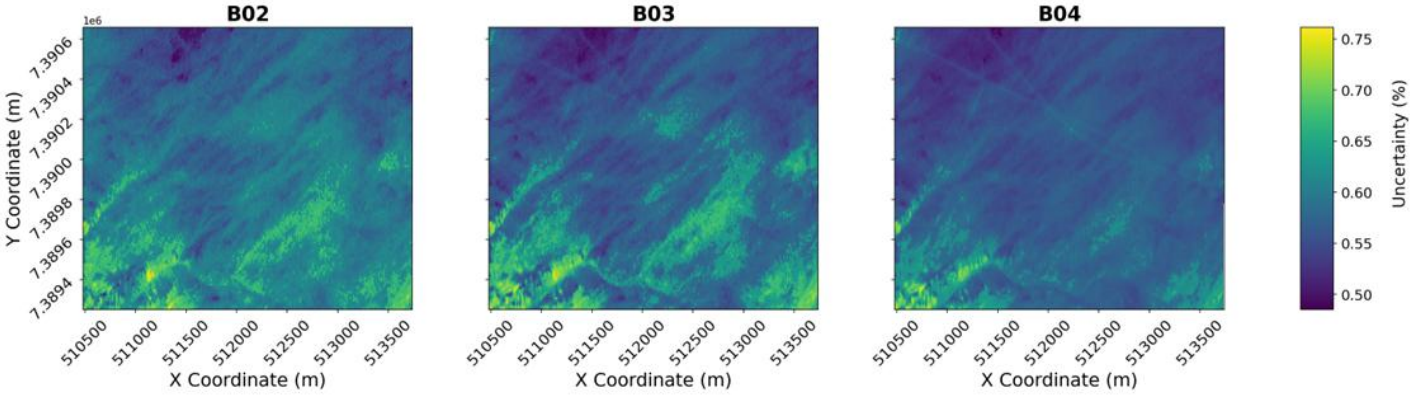


Figure 9 –Uncertainty due to sensor calculated using the Sentinel-2 Radiometric Uncertainty Tool (RUT) a for a given Sentinel-2 tile over the RCN GONA site in June 2024, for the RGB bands: 2, 3 and 4.

The errors relating to the satellite sensor calibration, for the TOA data used in these comparisons, arise from radiometric calibration. The particular calibration methods can vary from sensor to sensor but commonly include accounting for sensor degradation and calculating radiometric gain and bias values. The uncertainty attributed to sensor calibration should be well-defined in the satellite data provider's documentation.

Both satellite sensor noise and calibration effects are displayed in Table 5-1 below.

Table 5-1 – Effects table for satellite sensor uncertainties

Satellite Sensor Effects			
Name of effect		Satellite sensor noise	Satellite sensor calibration
Affected term in measurement function		$\rho_{\text{target,i}}(\lambda_b, t_{target})$	$\rho_{\text{target,i}}(\lambda_b, t_{target})$
Correlation type and form	Temporal (within site) (t)	Random	Systematic
	Band (within site) (b)	Random	Systematic
	Between sites (s)	Random	Systematic
Correlation scale	Temporal (within site) (t)	0	Mission lifetime
	Band (within site) (b)	0	Assume correlated between bands
	Between sites (s)	0	0
Uncertainty	PDF shape	Gaussian	Gaussian
	units	N/A	N/A
	magnitude	Sensor dependent, band dependent. Typical value: ~ 0.75 %	Sensor dependent, band dependent. Typical value: ~2-3 % for agency missions
Sensitivity coefficient		$\frac{\partial \overline{\rho}_{target}(\lambda_b, t_{target})}{\partial \rho_{\text{target,i}}(\lambda_b, t_{target})}$	$\frac{\partial \overline{\rho}_{target}(\lambda_b, t_{target})}{\partial \rho_{\text{target,i}}(\lambda_b, t_{target})}$

5.2 Reference Data Effects

This section describes the error effects associated with the reference in-situ data. For RCN, all uncertainties associated with the reference TOA reflectance data are encompassed by a single uncertainty value per band, provided with the product. The typical values for RCN uncertainties, displayed in Figure 10, are around 3 % for GONA site data, and around 4 % for RVUS site data, showing that this varies per site. Though the RCN Working Group states that for all the sites, after processing to TOA reflectance, it is typically 5% [RD-14].

For the TOA reference data used in these comparisons, uncertainties would arise from noise, sensor calibration and atmospheric correction and propagating the in-situ data from the ground to TOA reflectances. On the RCN portal, there is a detailed uncertainty budget for each site (called Uncertainty Statement) for BOA reflectances [RD-9]. Additional uncertainties regarding TOA processing are provided as part of the product, but there is no publicly available Uncertainty Statement for RCN TOA data with detailed parameterisation. However, the BOA statement for GONA includes a figure plotting the percentage uncertainty associated with TOA reflectance on a typical day, where values span ~ 1-8 % for wavelengths between ~ 450-1300 nm [RD-15]. The singular TOA reflectance uncertainty value per band for RCN products is displayed in Table 5-2 below. For the temporal correlation type, we assume systematic uncertainties dominate to avoid underrepresenting the overall uncertainty.

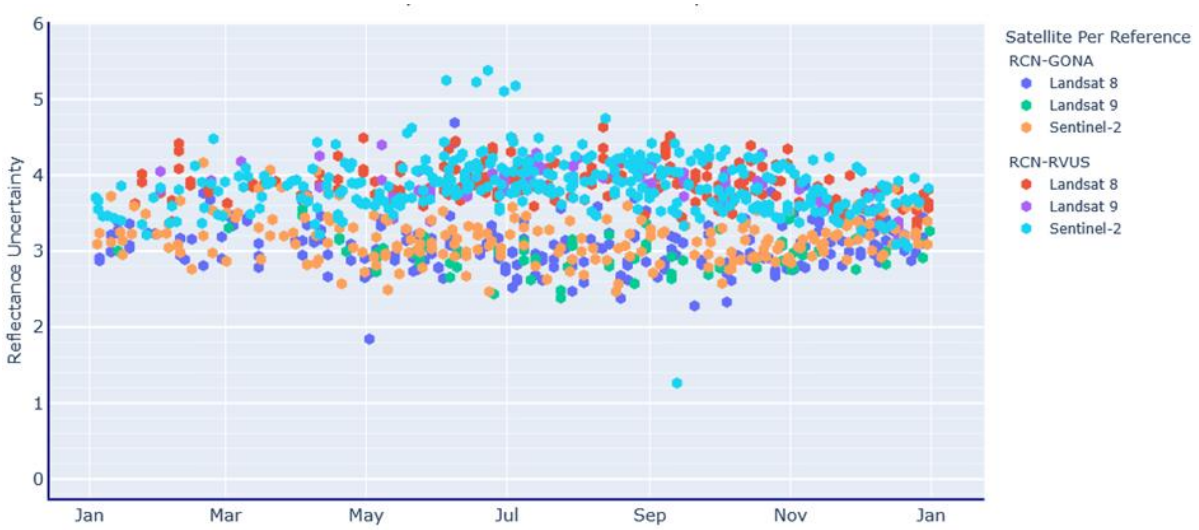


Figure 10 – RCN product uncertainties for both RCN sites: GONA & RVUS from matchups with Sentinel-2 and Landsat 8 and 9, between 2017-24 inclusive for the blue band.

Table 5-2: Effects table for reference data uncertainties

Reference Data Effects		
Name of effect		Reference data uncertainty
Affected term in measurement function		$\rho_{ref}(\underline{\lambda}, \underline{t})$
Correlation type and form	Temporal (within site) (t)	Not defined in product. Assuming systematic.
	Band (within site) (b)	Not defined in product. TBD
	Between sites (s)	Systematic
Correlation scale	Temporal (within site) (t)	0
	Band (within site) (b)	0
	Between sites (s)	0
Uncertainty	PDF shape	Gaussian
	units	Counts
	magnitude	Site and sensor dependent. Typical value: ~ 1-8 %
Sensitivity coefficient		$\frac{\partial \rho_{ref}(\lambda_b, \underline{t})}{\partial \rho_{ref}(\underline{\lambda}, \underline{t})}$

5.3 Comparison Process Effects

This section describes the error effects associated with the steps in the comparison process: spatial aggregation, observation geometry differences, temporal interpolation model used and band integration method applied.

5.3.1 Spatial Aggregation Method Effects

The RCN instrumented sites are chosen such that they are relatively homogeneous at the scale of satellite observations. Despite this, a mismatch still exists between the in-situ point measurement and the spatially integrated satellite measurement, due to the spatial heterogeneity of the site. This could be due a variety of sources including natural variability, e.g. vegetation, or artificial elements, such as roads and fences.

To quantify this effect, site heterogeneity is often characterised through a Spatial Homogeneity Index (SHI). SHI is calculated by normalising the standard deviation of high-spatial-resolution imagery of a particular ROI by the mean of the pixels in the ROI. SHI provides an estimate of this point-to-pixel mismatch uncertainty, given the field-of-view of the in-situ instrument is similar to that of the high-resolution imagery used to characterise it.

This analysis has been performed for Gobabeb using PlanetScope data captured over the HYPERNETS site in Gobabeb (GHNA). The SHI within the GHNA ROI (200 x 200 m) was calculated for a year of PlanetScope BOA reflectance data (spatial resolution 3 m), the results are displayed in Figure 11. Since the RCN GONA site is located around 650 m from the HYPERNETS GHNA site, the evaluated SHI value, 2%, is assumed representative of both sites and can be used as an uncertainty estimate for RCN comparisons. This analysis should be extended to the other RCN sites.

It is worth noting that this point-to-pixel mismatch uncertainty in principle could be reduced by developing a model to up scale the point measurements to better represent the satellite ROI. Both ROI spatial heterogeneity and spatial averaging method effects are displayed in Table 5-3 below, though the uncertainty estimate relating to the averaging method itself is still to be analysed.

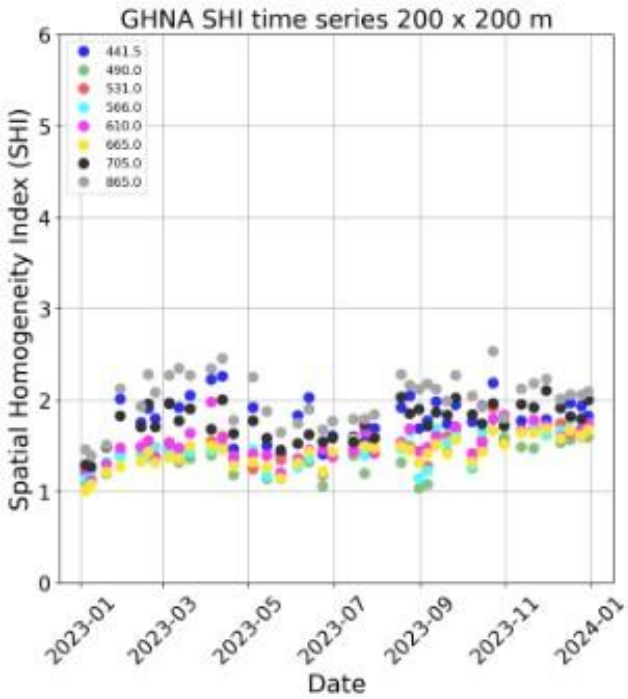


Figure 11 – Spatial Homogeneity Index (SHI) for PlanetScope BOA reflectance data and HYPERNETS GHNA in-situ data for 2023, for a 200 x 200 m ROI.

Table 5-3: Effects table for spatial aggregation uncertainties

ROI Spatial Aggregation Effects		
Name of effect		ROI spatial heterogeneity
Affected term in measurement function		$+0$
Correlation type and form	Temporal (within site) (t)	Systematic
	Band (within site) (b)	Random
	Between sites (s)	
Correlation scale	Temporal (within site) (t)	0
	Band (within site) (b)	0
	Between sites (s)	TBD
Uncertainty	PDF shape	Gaussian
	units	N/A
	magnitude	Typical value: ~ 2 %
Sensitivity coefficient		$u(0)$

5.3.2 Observation Geometry Difference Effects

The RCN in-situ data is provided for nadir viewing. The viewing geometry for the target satellite sensors can vary within the sensors their field-of-view (FOV), for example for Sentinel-2 this is ± ~ 10˚ – this can be larger for sensors on agile platforms that can perform off-nadir pointing to view the site. This mismatch, without correction, creates an uncertainty which is highly dependent on the observation characteristics of the sensor and the BRDF characteristics of the site. It is possible to correct the data for these differences based on a BRDF model of the site, though a residual error will remain. However, RCN does not provide enough site-characterisation information with the product in order for users to carry such a correction out.

As with other error effects, Landsat and Sentinel-2 observations of GONA are used as a case study to analyse the uncertainty associated with this effect. Sentinel-2 and Landsat observations of GONA in fact cover two representative scenarios – given that Landsat observations of GONA are almost nadir and Sentinel-2 measurements are at ~10˚. These case study results can therefore represent a broad range of comparisons and provides boundary level uncertainties for most sensors which have viewing angles within this range, but excludes those viewing at higher angles due to off-nadir pointing.

This analysis simulated TOA reflectances, between 2018-26, at different viewing geometries and calculated the bias between these and RCN data. These biases were calculated using the HYPERNETS BRDF model for the Gobabeb site [RD-16] and the libRadtran radiative transfer model [RD-21]. As inputs, viewing angles from the satellite product (nadir for Landsat) as well as atmospheric values provided with the RCN product were used. Therefore, the biases are purely due to the difference in viewing geometries between the satellite & RCN only.

Figure 12 and Figure 13 show the distribution of the simulated biases per band (where blue represents Landsat and orange, Sentinel-2) between the satellite and in-situ data. The shape of the distribution is affected by changes in solar angle over the year and these results show a notable error for off-nadir viewing sensors like Sentinel-2 – on average ~ 0.9 %, whereas for more nadir-viewing sensors, such as Landsat, the error is considerably smaller, 0.2 %.

It is not straightforward to estimate the uncertainty from these error simulations. The GUM states that measurements should be corrected for all known systematic effects, with any residual error distribution from the correction representing the uncertainty. However, for this specific effect, standard RCN users are unable to perform any correction due to lack of site characterisation information. Therefore, the approach here, according to the GUM guideline (Section 6.3.1 Note, p. 24) [RD-1], is to add these uncertainty estimates linearly, rather than the usual method, root sum of squares. See also, a similar example explained in the Sentinel-2 Radiometric Uncertainty Tool paper [RD-13].

This analysis should be extended to the other RCN sites. As stated above, this Gobabeb case study analysis was performed using a BRDF model for the site [RD-16] and to repeat the analysis for other sites, access to a BRDF model for them is required. Some sites and sensors observation scenarios are more sensitive to the effect – e.g., sites with high anisotropy and sensors with off-nadir viewing. Moreover, satellite sensor observation geometries can vary between sites, for example over RVUS, Sentinel-2 views from both ± ~ 10˚ depending on ascending or descending mode, meaning these observation geometry differences will have a much larger effect than Landsat which also views this site only at nadir.

The error relating to the uncertainty due to observation geometry differences, displayed in Table 5-4 below, is taken from the current Sentinel-2 analysis over GONA due to its larger observation range. The value is the mean of the means per band, ~ 0.932 %, and is to be added linearly. Unless the observation is explicitly known to be nadir within a few degrees this uncertainty will be used for all cases up to a view angle of 10 degrees.

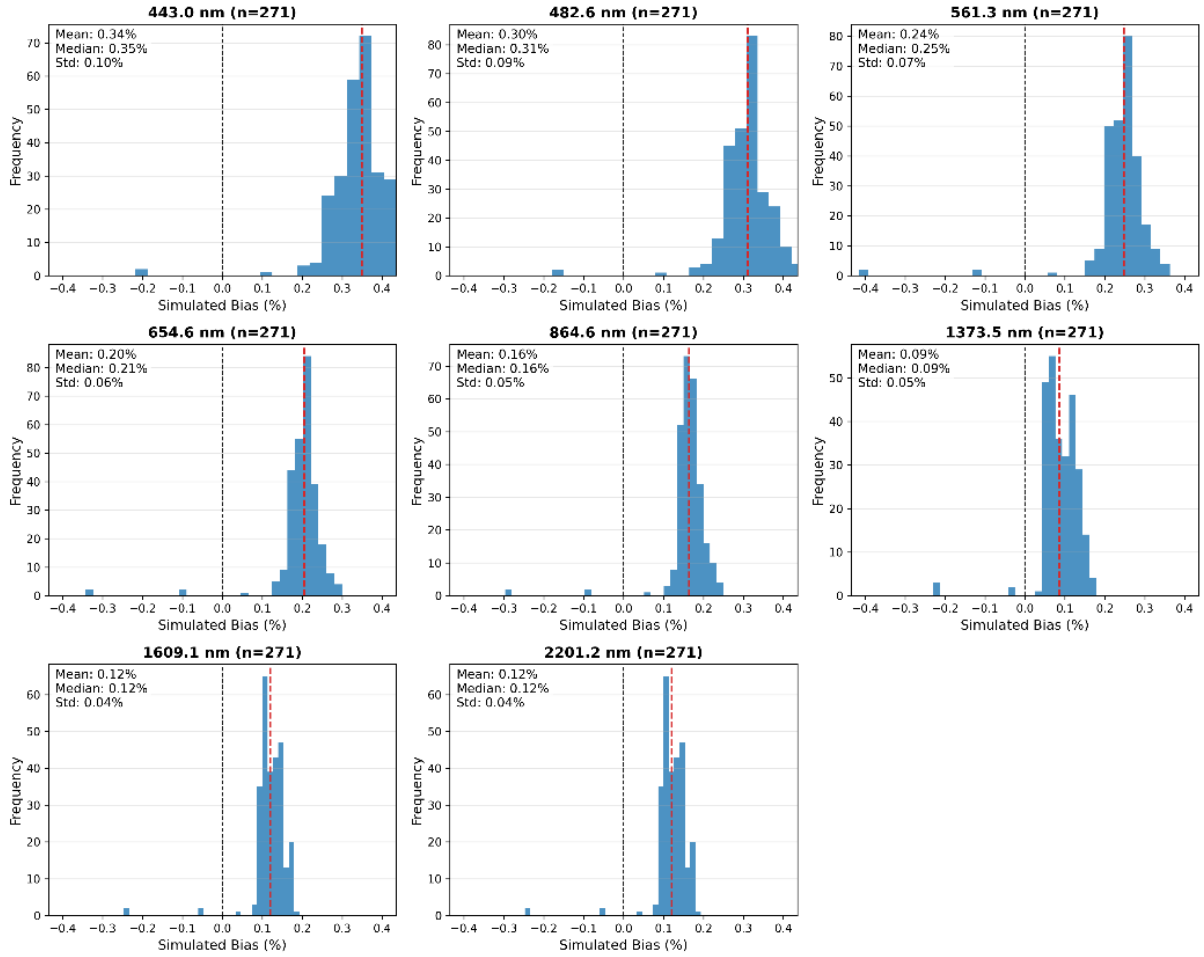


Figure 12 – Distribution of the simulated biases per band between Landsat 89 and RCN GONA in-situ data for 2018-26, where the bias is due to the difference in viewing angles between the satellite & RCN only.

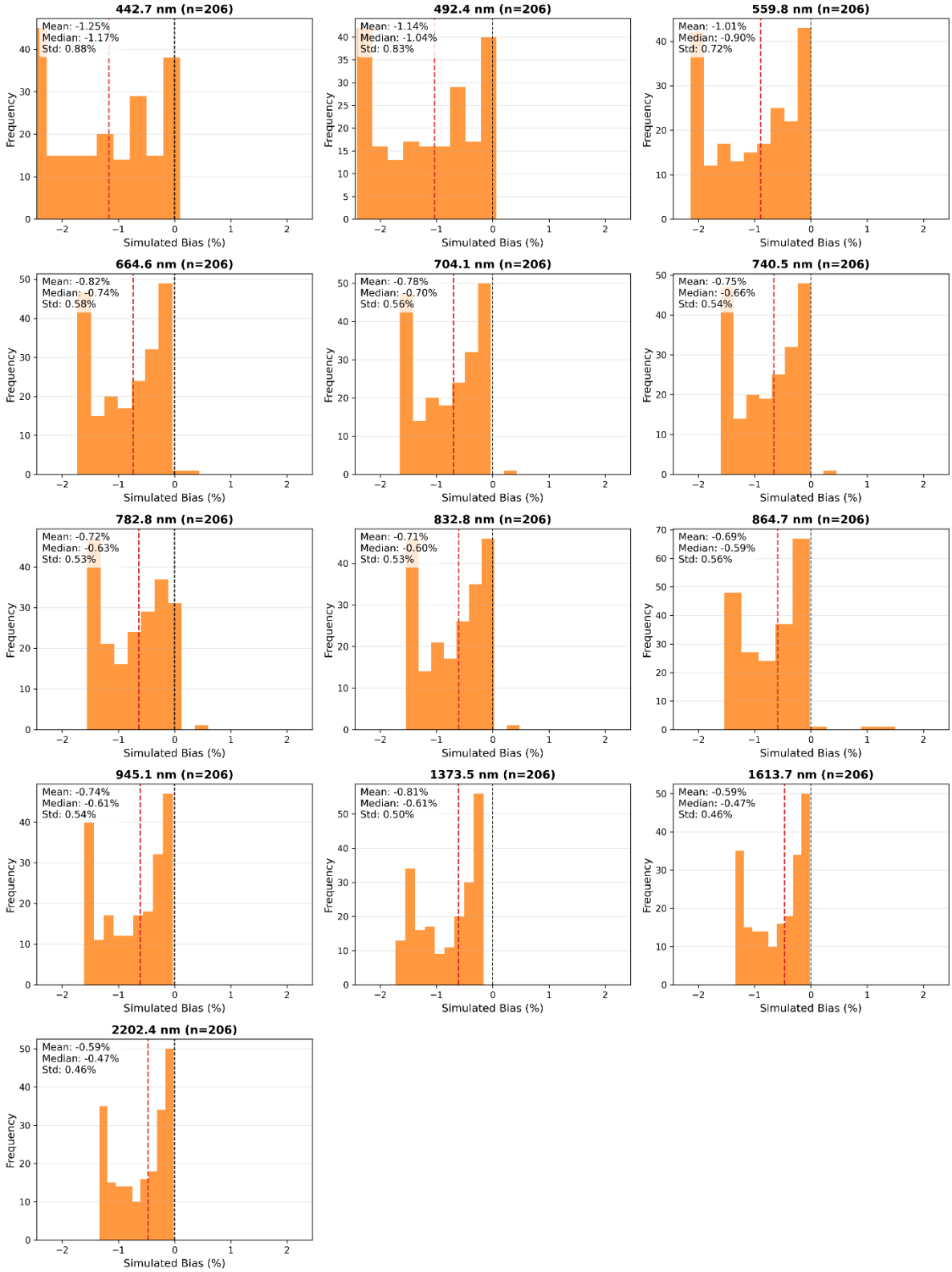


Figure 13 – Distribution of the simulated biases per band between Sentinel-2 and RCN GONA in-situ data for 2018-26, where the bias is due to the difference in viewing angles between the satellite & RCN only.

Table 5-4: Effects table for observation geometry differences uncertainties

Observation geometry Differences Effects		
Name of effect		Observation geometry differences
Affected term in measurement function		$+0$
Correlation type and form	Temporal (within site) (t)	Systematic
	Band (within site) (b)	Systematic
	Between sites (s)	Systematic
Correlation scale	Temporal (within site) (t)	0
	Band (within site) (b)	0
	Between sites (s)	0
Uncertainty	PDF shape	Top Hat
	units	N/A
	magnitude	Typical values (to be added linearly): Off-nadir: ~ 0.932 % Nadir-viewing: 0.2 % - see Figure 12 and Figure 13
Sensitivity coefficient		$u(0)$

5.3.3 Band Integration Method Effects

As explained in Section 4.1.2, spectral band adjustment is required to reconstruct the target sensor bands from in-situ observations. RadCalNet in-situ measurements are hyperspectral, which is intended to provide the capability to accurately match the spectral characteristics of multispectral target sensors. This is achieved by spectrally band integrating the hyperspectral reference data to the satellite bands.

The total uncertainty associated with spectral band integration is expected to arise from three main effects:

1. **Model error in the band integration process**, such as interpolation errors or numerical approximations used when aligning hyperspectral data with the sensor SRFs.
2. **Target sensor spectral calibration uncertainty**, arising from imperfect knowledge of the sensor SRFs – in particular wavelength knowledge.
3. **Finite spectral resolution of the reference data relative to the target sensor bands** – because the hyperspectral measurements do not sample the spectrum at infinitely fine resolution, narrow target bands may not be fully resolved, introducing uncertainty in the band-integrated values.

The magnitude of these effects varies by band and depends strongly on the underlying radiance/reflectance spectrum within that band. As a result, systematic biases may occur when comparisons are performed over scenes with consistent spectral features, as is the case when comparing over a single calibration site – or sites with similar characteristic, e.g., deserts. Both the sensor SRF and its associated uncertainties should be well-defined in the satellite data provider's documentation.

5.3.3.1 Target sensor spectral calibration uncertainty

A simulation study was performed to assess the uncertainty associated with the target sensor spectral calibration. Simulated observations were generated from 76 high-resolution surface reflectance spectra for a range of sandy/soil samples sourced from ECOSTRESS, USGS, and PICSAND spectral libraries [RD-20, RD-19, RD-18]. These spectra were propagated to TOA radiance using the *LibRadtran* radiative-transfer model under realistic atmospheric conditions [RD-21]. Wavelength-knowledge uncertainty is then propagated through the spectral band integration algorithm using a Monte-Carlo approach implemented in the open-source *CoMet* Toolkit [RD-17].

This analysis is demonstrated for the representative case study comparing multispectral Sentinel-2 MSI bands with hyperspectral RCN measurements over soil and sandy surfaces characteristic of e.g. the RCN GONA or RVUS calibration sites. This case study is considered broadly representative of multispectral sensor intercomparisons with hyperspectral in-situ data over desert sites, as the Sentinel-2 bands span a wide portion of the VNIR spectrum and are similar to those used across many operational multispectral imagers. Several commercial sensors - such as Planet SuperDove - also include spectrally aligned bands, making the findings directly applicable to a wider range of cross-sensor comparisons. The analysis should be extended for other surface types and sensors in future work, for a more comprehensive coverage.

Sentinel-2 MSI has a documented wavelength-knowledge uncertainty of 1 nm for all bands [RD-22] – wavelength errors are assumed here to be systematic across the spectral range.

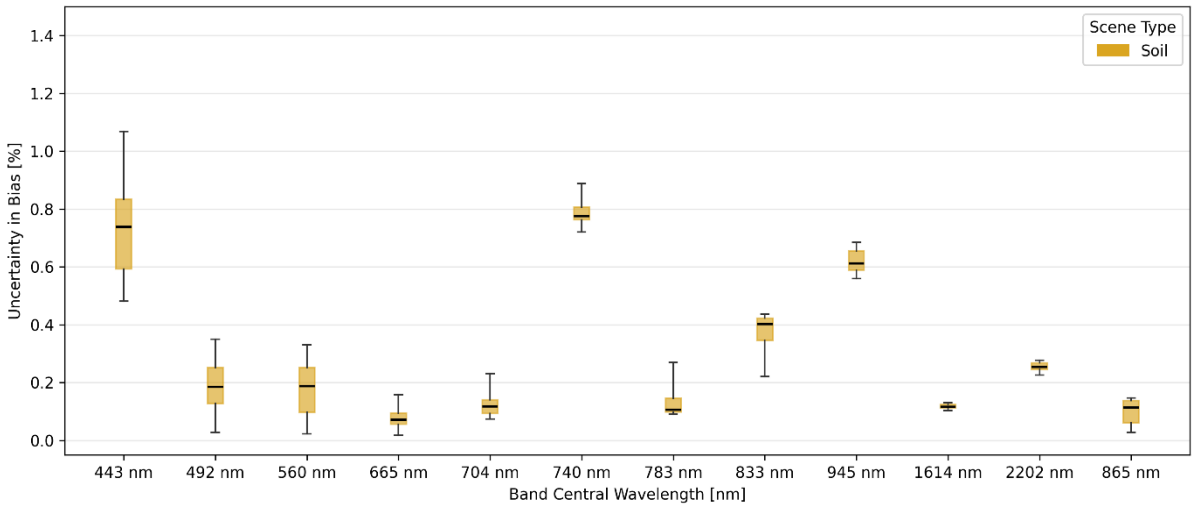


Figure 14 – Uncertainty bias percentage in the in-situ reference reconstructions of the MSI bands due to the 1 nm wavelength uncertainty.

Figure 14 presents the uncertainty in the in-situ reference reconstructions of the MSI bands due to the 1 nm wavelength uncertainty, with median uncertainties per band summarised in Table 5-5. For most bands, the resulting uncertainty is below 0.3 %, with larger values at 443 nm, 740 nm, and 945 nm which correspond with atmospheric absorption features and are therefore of reduced criticality for calibration with an in-situ reference. This uncertainty is treated as systematic between overpasses, as the spectral characteristics of the site remain relatively stable over time.

Table 5-5 - Uncertainty due to wavelength knowledge uncertainty of the target sensor, assuming a value for 1 nm (nominal value for Sentinel-2 MSI)

Band [nm]	**443**	**492**	**560**	**665**	**704**	**740**	**783**	**833**	**865**	**945**	**1614**	**2202**
Uncertainty [%]	0.74	0.19	0.19	0.07	0.12	0.78	0.11	0.40	0.11	0.61	0.12	0.26

5.3.3.2 Spectral resolution of the reference data

A further contribution arises from the finite spectral resolution and sampling of the RCN reference data, which limits how accurately the hyperspectral surface spectrum can be integrated through the sensor SRFs. This introduces a small residual bias – future implementations of this comparison framework could apply a correction based on this using high resolution spectra for each site, with an associated uncertainty. As with the geometry-mismatch-induced bias (see Section 5.3.2), this term is added linearly, not in quadrature, to the uncertainty budget.

The magnitude of this uncertainty is band-dependent, with negligible impact relative to the wavelength knowledge uncertainties presented in Table 5-5 above for the majority of bands. The impact is largest in or near absorption features, as expected, where coarse sampling fails to capture rapid spectral structure. Table summarises the evaluated uncertainty per band.

Table 5-6 - Uncertainty due to the spectral resolution of the RCN reference data over GONA-like desert/soil surface, showing per-band contributions – will be added linearly to the spectral-correction uncertainty budget.

Band [nm]	**443**	**492**	**560**	**665**	**704**	**740**	**783**	**833**	**865**	**945**	**1614**	**2202**
Uncertainty [%]	0.74	0.01	0.015	0.02	0.02	-0.86	0.79	0.01	0.00	-0.40	-0.07	0.00

5.3.3.3 Effects Table

The errors due to the band integration method, reference resolution and the satellite sensor SRF wavelength knowledge are displayed in Table 5-7 below.

Table 5-7: Effects table for band integration method uncertainties

Band Integration Method Effects			
Name of effect		Reference Resolution	Satellite sensor SRF wavelength knowledge
Affected term in measurement function		$+0$	$R_b(\lambda)$
Correlation type and form	Temporal (within site) (t)	Systematic	Systematic
	Band (within site) (b)	Band/scene-dependent. Less correlated between bands covering different spectral domains. High correlation between e.g. clustered red edge bands	Band/scene-dependent. Less correlated between bands covering different spectral domains. High correlation between e.g. clustered red edge bands
	Between sites (s)	Surface-dependent – systematic between surface types with consistent spectral characteristics	Surface-dependent – systematic between surface types with consistent spectral characteristics
Correlation scale	Temporal (within site) (t)	0	0
	Band (within site) (b)	0	0
	Between sites (s)	TBD	TBD
Uncertainty	PDF shape	Top Hat	Top Hat
	units	N/A	N/A
	magnitude	Band dependent – see Table 5-6. Typical value (to be added linearly) for RGB bands < 0.05 %	Band dependent – see Table 5-5. Typical value: ~ 0.2 %
Sensitivity coefficient		$u(0)$	$\frac{\partial \rho_{ref}(\lambda_b, \underline{t})}{\partial R_b(\lambda)}$

5.3.4 Temporal Interpolation Model Effect

As explained in Section 4.1.2.2, there are small differences between the time of the satellite overpass and reference in-situ measurement acquisition. These differences will be accounted for via temporal interpolation, which introduces residual error.

To investigate the scale of this residual interpolation error, we compared varying temporal interpolation models (e.g., difference between linear, cubic and quadratic interpolation). The *CoMet* toolkit *comet_maths* package [RD-17] has functionality that enables uncertainty estimation when comparing different temporal interpolation methods. This was run for RCN TOA reflectance data for six RCN wavelengths at three different target times for interpolation between the RCN data timestamps: no difference, 7.5-minute difference and 15-minute difference between the RCN time and the target sensor time. Note that the 15-minute difference is equidistant from two RCN data acquisition times, as the data is collected every 30 minutes. Figure 15 shows the results for two dates in both 2022 and 2024 and as expected, for no time difference the model percentage uncertainty is 0, and the percentage uncertainty increases with the time interval. The November 2024 data have the highest uncertainties, however overall, the percentage uncertainty remains below ~ 0.073 %. This shows that very little uncertainty is introduced due to residual error of the temporal interpolation model (negligible compared to other sources).

This highest value, relating to the largest time difference and therefore worst-case scenario, is used to quantify the uncertainty in the effects table, Table 5-8 below, alongside the other effect information.

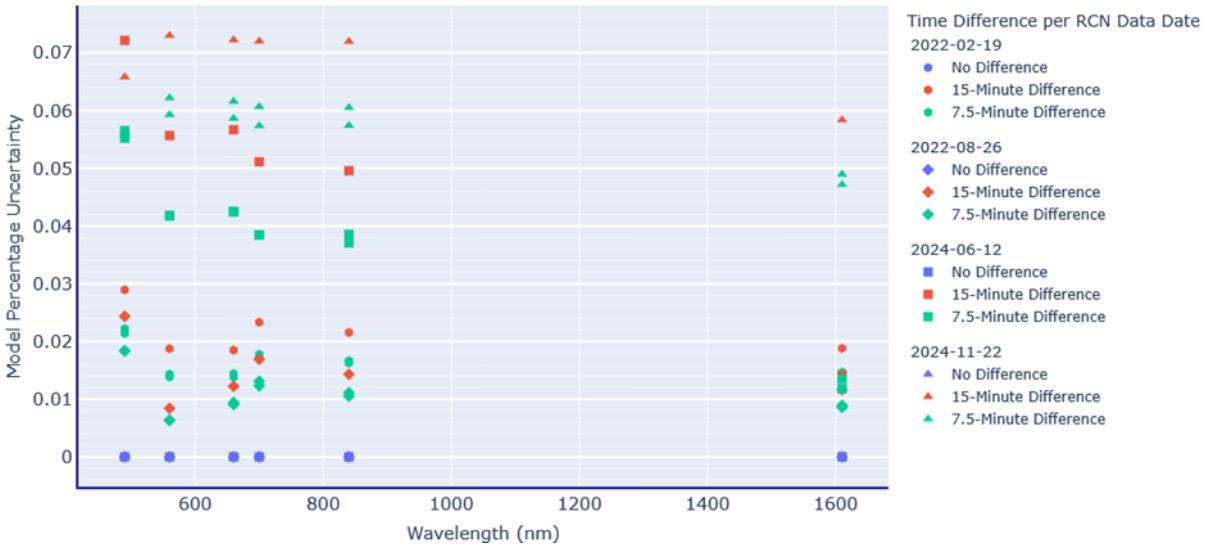


Figure 15 – Uncertainty due to varying interpolation methods (linear, cubic and quadratic), for six RCN wavelengths. Using RCN TOA reflectance data from two dates in 2022, and two dates in 2024, and calculating the uncertainty for various time differences from the RCN acquisition times.

Table 5-8: Effects table for temporal interpolation model uncertainties

Temporal Interpolation Model Effect		
Name of effect		Temporal interpolation model
Affected term in measurement function		$+0$
Correlation type and form	Temporal (within site) (t)	Systematic
	Band (within site) (b)	Systematic
	Between sites (s)	Random
Correlation scale	Temporal (within site) (t)	0
	Band (within site) (b)	0
	Between sites (s)	0
Uncertainty	PDF shape	Gaussian
	units	N/A
	magnitude	~ 0.073 %
Sensitivity coefficient		$u(0)$

5.4 Combining the comparison uncertainties

All the uncertainty estimates within this section combine to represent the total uncertainty arising from these multispectral satellite-to-in-situ comparisons. These are to be added in quadrature, except for the effects arising from the observation geometry difference and reference resolution, which following the GUM guideline (Section 6.3.1 Note, p. 24) [RD-1], will be added linearly. Table 6-1 in Section 6 shows an overview of all these uncertainty estimates; the final row states the total uncertainty, split into nadir-viewing and off-nadir-viewing missions, as for these scenarios two different estimates are added linearly.

For use in the CEOS-PVP, the uncertainties due to satellite calibration and reference data reflectance uncertainty are not included in the total; the reference data uncertainties are provided per reflectance within the RCN product and are therefore added dynamically and the satellite calibration uncertainty is dependent on the mission used as the benchmark for monitoring the mission's performance. Note that these uncertainties can be split into systematic and random, so when averaging over a timeseries of comparisons, the random uncertainties will reduce by the square root of the number of comparisons.

6 Discussion

The effects tables in Section 5 make up the initial version of this uncertainty budget for comparisons between RCN in-situ and multi-spectral satellite measurements. Table 6-1 summarises the current uncertainty estimates for each component of the budget. These results were reached through representative case studies, primarily with the RCN Gobabeb (GONA) site but also RVUS where possible. The Sentinel-2 and Landsat missions were used in many of the case studies as typically these are representative for many optical EO missions. For example, when analysing uncertainties due to the observation geometry, Sentinel-2's viewing geometry of ~10˚ and Landsat's nadir, provided an apt scope for understanding the extent of this error effect.

The uncertainty components associated with the satellite and reference data are stated by the provider and are therefore require no further steps. However, those associated with the comparison processing are currently of differing levels of maturity and can be developed further. The following subsections describe planned further analysis that aims to broaden the scope of each approach. In some cases, the current scope focuses on a single case study, between one satellite against one reference, and the goal is to eventually extend the analysis to a more a generalised approach, encompassing comparisons between any sensor against any RCN site. Any further analysis would enable an even more detailed understanding of the contributing uncertainties to multispectral satellite-to-in-situ comparisons.

Table 6-1 Current analysis maturity for each uncertainty component highlighted in Section 5

Category	Uncertainty Component	Source of Uncertainty Magnitude	Uncertainty Magnitude	Varies as a Function of	Current Maturity
Satellite	Noise	Provider	Sensor dependent, band dependent, provided by data provider. Typical value: ~ 0.75 %	Sensor performance	Operational (depending on mission)
	Calibration	Provider	Sensor dependent, band dependent, provided by data provider. Typical value: ~2-3 % for agency missions	Sensor calibration	Operational (depending on mission)
Reference Data	Reflectance uncertainty (encompassing all: noise, calibration, etc)	Provider	Site and sensor dependent, provided by data provider, RCN. Typical value: ~ 5%	Standard	Operational
Comparison	ROI spatial heterogeneity	Analysis	Typical value: ~ 2 %	Sensor spatial resolutions; site	Completed analysis for Gobabeb
	Observation geometry differences	Analysis	Observation geometry dependent. Typical values (to be added linearly): Off-nadir (<10°): ~ 0.9 % Nadir-viewing: 0.2 % - see Figure 12 and Figure 13	Sensor orbit track; site (BRDF model)	Completed analysis for representative case study, Landsat and Sentinel-2 comparisons with one RCN site, GONA
	Band integration – Reference resolution	Analysis	Band dependent – see Table 5-6. Typical value for non-absorption bands (to be added linearly): < 0.05 %	Reference sensor bands; site	Completed analysis for desert/soil surfaces (i.e., RCN GONA, RVUS)
	Band integration – Satellite sensor SRF wavelength knowledge	Analysis	Band dependent – see Table 5-5. Typical value: ~ 0.2 %	Satellite/target sensor bands	Completed analysis for representative mission, Sentinel-2 (would apply to equivalent bands on other satellites, e.g. Landsat-89 OLI)
	Temporal interpolation model	Analysis	~ 0.073 %	Sensor overpass time	Completed analysis for RCN GONA
	Total uncertainty (including satellite calibration & reference data reflectance uncertainty):		7.2 % (off-nadir-viewing missions) 6.5 % (nadir-viewing missions)		